Marc, O., Hovius, N., Meunier, P. (2016): The mass balance of earthquakes and earthquake sequences. - *Geophysical Research Letters*, *43*, 8, pp. 3708–3716.

DOI: http://doi.org/10.1002/2016GL068333

AGU PUBLICATIONS

Geophysical Research Letters

RESEARCH LETTER
10.1002/2016GL068333

Key Points:
- Earthquake mass balance based on a seismologically consistent expression of coseismic landsliding and Okada's surface deformation solution
- Large earthquakes are always constructive, while intermediate ones may be erosive if shallow enough and below a steep enough topography
- Earthquake sequences on fault smaller than 120 km may limit topography building especially if they follow a Gutenberg-Richter distribution

Supporting Information:
- Supporting Information S1
- Figure S1

Correspondence to:
O. Marc,
omarc@gfz-potsdam.de

Citation:
Marc, O., N. Hovius, and P. Meunier (2016), The mass balance of earthquakes and earthquake sequences, *Geophys. Res. Lett.*, *43*, 3708–3716, doi:10.1002/2016GL068333.

Received 19 FEB 2016
Accepted 5 APR 2016
Accepted article online 8 APR 2016
Published online 27 APR 2016

The mass balance of earthquakes and earthquake sequences

O. Marc[1,2], N. Hovius[1,2], and P. Meunier[3]

[1]Helmholtz Centre Potsdam, German Research Center for Geosciences, Potsdam, Germany, [2]Institute of Earth and Environmental Science, Potsdam University, Potsdam, Germany, [3]Laboratoire de Géologie, École Normale Supérieure de Paris, Paris, France

Abstract Large, compressional earthquakes cause surface uplift as well as widespread mass wasting. Knowledge of their trade-off is fragmentary. Combining a seismologically consistent model of earthquake-triggered landsliding and an analytical solution of coseismic surface displacement, we assess how the mass balance of single earthquakes and earthquake sequences depends on fault size and other geophysical parameters. We find that intermediate size earthquakes (M_w 6–7.3) may cause more erosion than uplift, controlled primarily by seismic source depth and landscape steepness, and less so by fault dip and rake. Such earthquakes can limit topographic growth, but our model indicates that both smaller and larger earthquakes ($M_w < 6$, $M_w > 7.3$) systematically cause mountain building. Earthquake sequences with a Gutenberg-Richter distribution have a greater tendency to lead to predominant erosion, than repeating earthquakes of the same magnitude, unless a fault can produce earthquakes with $M_w > 8$ or more.

1. Introduction

At the Earth's surface, geological processes creating topographic relief compete with geomorphic processes that level it. Where crustal deformation is rapid, shallow earthquakes can dominate the displacement of rocks and the surface [*Avouac*, 2007], and overlying topography can grow over a succession of seismic cycles [*King et al.*, 1988; *Le Béon et al.*, 2014; *Simpson*, 2015]. In the steep landscapes that prevail in such areas, shallow earthquakes can also induce widespread landsliding [e.g., *Keefer*, 1994] by short-lived, cyclic changes of the normal and shear stresses in hillslopes due to strong ground motion, shattering of the bedrock, and rapid changes in groundwater distribution. In active mountain belts most valleys contain only small amounts of sediment, suggesting that, over multiple seismic cycles, most landslide debris is evacuated. Therefore, erosion due to landslides should be included in the mass balance of an earthquake. Here the volume balance of an earthquake is defined as the difference between the change in rock volume above a reference plane (e.g., sea level) due to coseismic surface deformation and the volume of surface material mobilized by seismically induced mass wasting and subsequently removed from the landscape, adjusted for the local effects of isostatic compensation. Assuming a homogeneous density of 2600 kg m^{-3} for the eroded and uplifted rocks, the mass balance can be derived from the volume balance. Strictly, this mass balance pertains to the area located above or in the direct vicinity of shallow faults that are locked during most of the seismic cycle, where seismic deformation is predominant. To keep a simple and analytical approach, we have not included the effect of interseismic strain near the fault.

Recent studies suggest that the mass balance differs between earthquakes. Despite intense mass wasting, the 1999 M_w 7.6 Chi-Chi earthquake in Taiwan caused growth of the hanging wall topography [*Hovius et al.*, 2011], but landsliding due to the 2008 M_w 7.9 Wenchuan earthquake in China matched seismic surface uplift [*Parker et al.*, 2011; *Li et al.*, 2014]. *Barlow et al.* [2015] showed that tectonic subsidence was much greater than topographic lowering due to seismically induced mass wasting for the 2010 M_w 7.2 El Cucapah Mayor earthquake. *Li et al.* [2014] also developed a more general treatment of the balance of seismically induced landsliding and uplift, assuming that the rate of landsliding scales linearly with earthquake moment [*Keefer*, 1994]. Notably, they predicted that earthquakes larger than a critical magnitude (~M_w 8) would systematically have more erosion than uplift. If correct, this would have significant consequences for the emergence and growth of mountain ranges due to seismic processes. However, consideration of the spreading and attenuation of seismic waves with increasing distance from their earthquake source, and the geometry of faults likely to produce earthquakes of different magnitudes, suggests that the landslide rate is nonlinear in earthquake moment [*Marc et al.*, 2016]. Moreover, beside the influence of local

climate [*Barlow et al.*, 2015], the amount of landsliding due to a given earthquake is limited by the area that can fail, as well as by the imposed seismic trigger. Tested against a comprehensive compilation of estimates of earthquake-induced landslide volumes, the seismologically consistent model of *Marc et al.* [2016] performed better than any direct fit between earthquake moment and estimated landslide volume. We consider that this new model provides, for the first time, a robust basis for comparison with the coseismic uplift volume, which can be computed for any given earthquake from the surface deformation field using the approach of *Okada* [1985].

Marc et al. [2016] derived and calibrated a seismologically consistent expression for the total volume of landslides caused by earthquakes but did not compare it to the surface deformation associated with earthquakes. Here we explore the parameters controlling the mass balance of earthquakes with a thrust component, combining the approaches of *Marc et al.* [2016] and *Okada* [1985]. In addition, we investigate the evolution of this mass balance for a fault experiencing many earthquakes over the long term. We finish by discussing the implications of our results for the topographic evolution of fault-bounded structures and for mountain building.

2. Methods

2.1. Uplift Modeling

Okada [1985] has developed an analytical solution for the surface displacement produced by slip on a plane in an elastic infinite half space. The surface displacement vector orientation depends mainly on the dip and rake of the rupture patch, while its norm is strongly dependent on the depth of the patch and the amount of slip. The vertical displacement caused by a thrust fault forms a dome of absolute uplift, with an extent scaling with the size and centroid depth of the fault, surrounded by two subsiding lobes (Figure S1 in the supporting information). This solution requires specification of the rupture patch dimensions (length and width), geometry (strike, dip, and depth centroid), and the amount of slip. We derived length, L, width, W, and average slip, D, from fault scaling relationships with seismic moment, Mo, [*Leonard*, 2010] and obtained the total uplifted volume, V_u, for earthquake scenarios by numerically integrating all vertical surface displacement $>0.5\%$ of the maximum, thus accounting for near-field subsidence at the periphery of uplift areas (supporting infomation Sl). The modeled uplifted volume V_u is approximately proportional to the earthquake moment and independent of the fault centroid depth, as the large increase in the total uplifted area with increasing centroid depth is balanced by the decrease in maximum surface displacement (supporting infomation Sl). The main parameters determining the uplifted volume are, therefore, the earthquake moment, Mo, the dip, d, and the rake, r, of the fault (Figure 1). At $d = 45°$ and $r = 90°$ the amount of subsidence relative to uplift due to earthquake slip is minimized, and V_u is maximized. V_u decreases as d departs from 45°, tending to zero (with subsidence canceling uplift) when r tends to zero or 180 (strike slip) and becomes negative with net subsidence when r is negative (normal fault).

2.2. Landslide Modeling

Complementing the surface displacement model, we have used a seismologically consistent model predicting the total volume of landslides triggered by an earthquake, Vp, as a function of seismic moment, asperity mean depth, $R0$, and landscape modal slope, $Smod$ [*Marc et al.*, 2016, Figure 1]. The modal slope is easily extracted from a digital elevation model and appears to be a good proxy for the abundance of steep terrain (>30–40°) prone to landsliding and therefore a first-order indicator of the landscape-scale propensity to failure [*Marc et al.*, 2016] This model derives from explicit consideration of processes modulating the peak ground acceleration that controls landsliding [*Khazai and Sitar*, 2004; *Meunier et al.*, 2007, 2013; *Yuan et al.*, 2013], such as the amplitude of high-frequency waves emitted at the source and the wave attenuation due to geometric spreading. In our model, the critical magnitude, above which an earthquake causes discernable landsliding and Vp assumes a nonzero value, is modulated by $R0$ and ranges between M_w 5 and 6 (Figure 1). Above this critical magnitude, Vp rises sharply, driven by the exponential increase of the ground shaking with increasing earthquake moment and by rupture length increase. Strong-motion observations show that the peak ground acceleration caused by an earthquake stop to increase with moment magnitude at what is termed the hinge magnitude, $M_wh = 6.75$ [cf. *Boore and Atkinson*, 2008; *Baltay and Hanks*, 2014]. Above this magnitude, Vp increases principally due to the growth of rupture length with moment, $Vp \sim L \sim Mo^{2/5}$ [cf. *Marc et al.*, 2016] (Figure 1). This model differs from the classic,

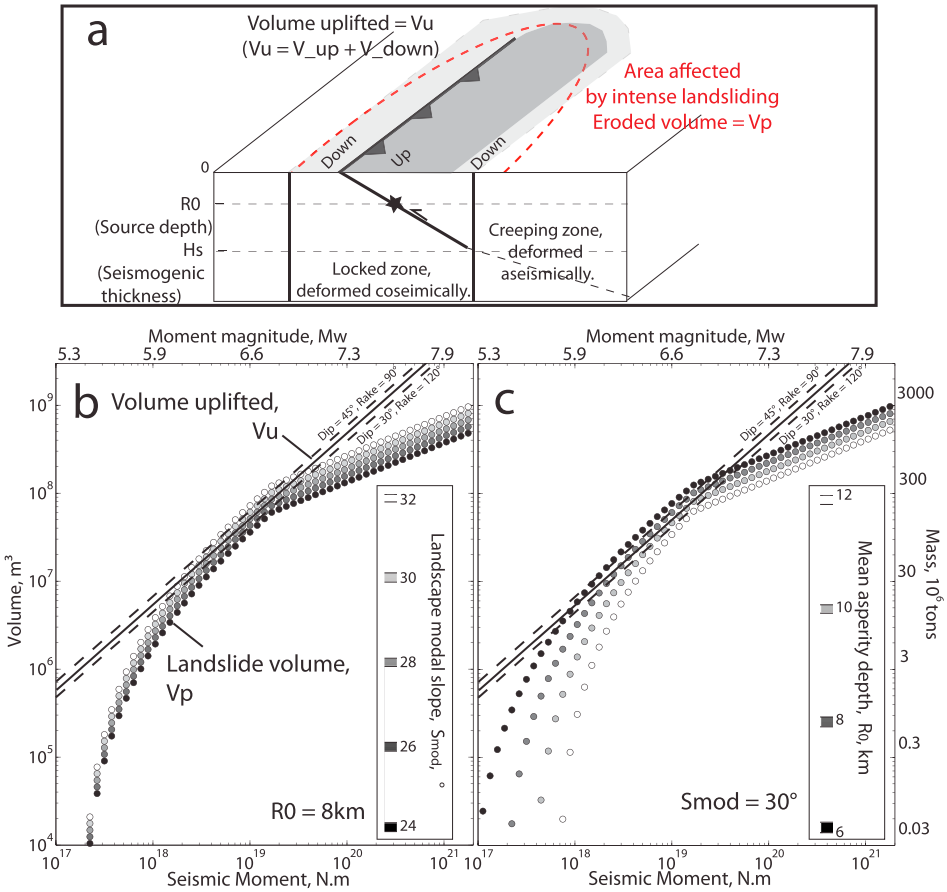

Figure 1. Sketch of the uplift and erosion caused by an earthquake above its (a) causative fault and coseismic uplifted volume (Vu) and coseismic eroded volume through landsliding (Vp) against seismic moment for earthquakes with (b) different landscape modal slope and (c) different asperity depth. Equivalent mass when assuming a homogeneous rock density of 2600 kg m^{-3} is indicated on the right *y* axis. In Figures 1b and 1c, the solid and two dashed lines represent the uplifted volume for an earthquake on a 30° dipping fault, with 90° rake, a 45° dipping fault, with 90° rake, and a 30° dipping fault, with 120° rake.

empirical relationship proposed by *Keefer* [1994], in which landslide volume increases linearly with earthquake moment.

The landslide model has been shown to be more accurate than empirical relationships, with predicted landslide volumes within a factor of 2 of independent estimates for earthquakes with magnitudes between 5 and 8 in two thirds of 40 documented cases [*Marc et al.*, 2016]. However, it has been found to overpredict landslide volumes where exceptionally strong lithologies, such as massive carbonates, are present, and for earthquakes with complex rupture mechanisms, such as supershear.

3. Mass Balance of Single Earthquakes

The mass balance of earthquakes is found as the ratio of the curves for total uplift and total landsliding. Here we explore the role of earthquake magnitude and the effects of source depth and landscape steepness, which modulate landsliding, and of dip and rake which modulate the uplifted volume.

For a given fault geometry, the uplift term increases almost linearly with the seismic moment, but the relation between landsliding and the seismic moment is more complex. In small earthquakes, the ground shaking is insufficient to cause substantial landsliding and uplift always dominates. However, above the threshold for

slope failure, the landslide term increases much faster with moment than the uplift term, up to the hinge magnitude, $Mh = 6.75$. Beyond this magnitude, the landslide volume scales with moment to the power 2/5, and triggered landslide volume increases much slower than the uplift volume. Therefore, for a given source depth and landscape steepness, the landslide volume may exceed the uplifted volume around the $Mh = 6.75$, and intermediate size earthquakes, with M_w 6 to 7, may have a negative mass balance (Figure 1). But for large earthquakes we find, in contrast to *Li et al*. [2014], that the net surface uplift always exceeds the expected landsliding (Figure 1).

The range of earthquake magnitudes with a negative mass balance is strongly controlled by the source depth and landscape steepness and is smallest for earthquakes rupturing at greater depth or below gentle topography. For example, according to our model, an earthquake with source at 8 km or deeper below topography with modal slope less than 23° will never be erosive (Figure 1b). Even in very steep landscapes with modal slope of 32°, earthquakes deeper than 14 km will never be erosive (Figure 1c). These considerations apply to a thrust fault with a dip of 30° and pure dip slip (rake = 90°). The net surface uplift would be reduced if the rake increased or the dip decreased (Figure 1), affecting the earthquake mass balance. For example, shallow earthquakes on a fault with dip of 15° and a rake of 120° could still have excess erosion at $M_w \sim 7.3$. However, for values consistent with thrust earthquakes (i.e., $120° > \text{rake} > 60°$ and $10° > \text{dip} > 45°$) these parameters have limited importance compared to topographic steepness and source depth (Figure 1). In summary, our results indicate that the mass balance of earthquakes depends critically on the earthquake characteristics and that above a certain magnitude, uplift always dominates. For a given earthquake the typical uncertainty (which applies in about two thirds of cases documented in *Marc et al.* [2016]) of the total landslide volume predicted by the model we use here is about a factor of 2 [*Marc et al*., 2016], meaning that even for a M_w 6.8 event, for which the landslide volume is largest relative to uplift, uplift and erosion are the same within error for most earthquake settings (Figure 1).

4. Mass Balance of Earthquake Sequences

We have explored the effects of different physical parameters on the mass balance of single earthquakes. However, growth of fault-controlled structures and mountain ranges occurs over many earthquake cycles [*King et al*., 1988]. To assess the long-term mass balance of the locked portion of a seismogenic fault, we have modeled two end-member scenarios. One is a fault dominated by repeating earthquakes of characteristic magnitude. The other is a fault rupturing in earthquakes of various magnitudes on random subsegments. In this second scenario, we assume that the distribution of earthquake magnitudes follows a Gutenberg-Richter relationship [*Gutenberg and Richter*, 1954], described by a power law decay with exponent ~1, with at least one earthquake of maximum magnitude, M_wX, rupturing the entire fault. The Gutenberg-Richter relationship applies at regional scales and may hold for some fault system, for example, for the Himalayan front [*Avouac*, 2015]. Even if it is not clear to which extent these scenarios are realistic, they represent plausible end-members likely encompassing the behavior of most major fault systems.

For these two scenarios, the long-term mass balance of a seismogenic structure, defined as the cumulative volume change, is obtained by summing the erosion and uplift caused by all earthquakes on the structure with $5 < M_w < M_wX$. When considering a Gutenberg-Richter scenario we have normalized this cumulative volume change by the fault area, obtaining a cumulative elevation change, and allow for easier comparison between events. In this calculation, the effects of smaller earthquakes, $M_w < 5$, are neglected because our model predicts little or no landsliding for such events in most settings and because the long-term surface uplift is dominated by the largest events. The variations or evolution of other model parameters over the long term must also be constrained. In many active mountain belts, convergence rates are sufficient to produce several dozens of characteristic earthquakes, or a few thousands of earthquakes following a Gutenberg-Richter distribution over time scales of 10^5 year, short compared to the structural evolution of a mountain belt and short enough to neglect viscous behavior of the crust. Thus, it is reasonable to assume that the fault geometry and rupture mode remain fairly constant over this period and that we can use mean values of dip and rake angle. Moreover, we keep M_wX fixed and neglect any fault growth; therefore, our calculations are best suited to relatively large and mature faults, the rupture width and length of which are constrained by structural discontinuities. Climate and erosional conditions acting on the landscape may change importantly over such time scales, but for simplicity we assume a constant topographic slope distribution.

Finally, the distribution of asperity depths over the long term must be considered. For a seismogenic layer of thickness Hs and a fully locked fault (i.e., moving only in earthquakes), the cumulative seismic slip on the fault must be uniform over the full depth range and is set by the convergence rate. This is important because the landslide volume assigned by our model is very sensitive to the depth of the zone of largest slip [*Meunier et al.*, 2013, *Marc et al.*, 2016], or asperity, that emits most of the high-frequency waves-triggering landslides [*Ruiz et al.*, 2011; *Avouac et al.*, 2015]. Therefore, long-term mass balance calculations depend critically on the depth range over which all earthquakes are distributed equally in order to satisfy equal slip. This range is set between the surface (1 km depth for numerical convenience) and Hs, typically between 15 and 20 km [*Leonard*, 2010]. Additionally, for a given dip angle and seismogenic thickness there is a critical earthquake magnitude beyond which the width of the rupture cannot increase. This mechanical boundary yields a break in rupture size scaling, which is clearly observed for strike-slip faults [*Leonard*, 2010], but not for dip-slip faults, suggesting that, in general, very large dip-slip earthquakes may not reach down the base of the seismogenic layer because the fault has a low dip angle or a flat and ramp geometry.

Hence, our calculations of the long-term mass balance of seismogenic faults depend on the fault geometry, fault length or maximum earthquake magnitude, and the thickness of the seismogenic layer. Here our analysis cannot be exhaustive with respect to the range of geometries. Instead, we consider three typical settings. The first is a textbook thrust dipping at 30°. The second is a thrust gently dipping at 15°, as representative of the geometry of megathrusts in the Himalayan range. The third fault has a flat and ramp geometry, with a ramp dipping at 30° and a flat dipping at 10°, as can be found in fold and thrust belt settings. The flat is set to have 3 times the width of the ramp, with a transition between the two segments at a constant depth of 8 km, and with a variable ratio of aseismic over seismic slip (supporting information S1).

5. Long-Term Mass Balance of Faults

In the first end-member scenario, repeating earthquakes with a constant magnitude and geometry occur on a fault. The main difference with respect to a single earthquake is that to maintain equal slip on the locked portion of the fault, earthquakes must rupture asperities at all depths, and the thickness of the seismogenic layer becomes the relevant parameter in the long term. For large events, the cumulative landsliding of N earthquakes distributed through depth is similar to N times the landslide volume of a single earthquake occurring at a characteristic depth of approximately half the thickness of the seismogenic layer (Figure 2). Earthquakes larger than $M_w \sim 7.0$ or $M_w \sim 7.3$ are constructive, even under steep landscapes, for 30° dipping faults or gently dipping and flat and ramp faults, respectively (Figure 2). For smaller earthquakes, the scaling of the landslide volume with earthquake moment is different because when distributed over depth even very small earthquakes ($M_w < 5$) will trigger some landsliding (Figure 2b). The transition between these two regimes occurs between M_w 6 and 6.5 when earthquakes at the base of the seismogenic layer are expected to cause ground shaking which does not exceed the threshold for landsliding. In either case, the standard deviation of the cumulative landslide volume caused by N earthquakes of equal magnitude is the one of a single earthquake divided by the square root of N. For a sequence of 25 earthquakes the standard deviation on the long-term cumulative volume would be ~20%. This uncertainty estimate assumes a normal distribution of errors, which may not be reasonable for special cases dominated by very large rock strength or peculiar seismic ruptures [*Marc et al.*, 2016].

As a second end-member scenario, we consider a sequence of earthquakes with magnitudes distributed according to the Gutenberg-Richter relation, where the many small and intermediate earthquakes may have a different effect on the topography than the rare, large earthquakes. Notably, because the exponent on the earthquake frequency-magnitude distribution is one, or two thirds in moment, the surface uplift, which is linear in moment, is controlled by the largest earthquakes. However, the landslide model has a break in scaling with seismic moment at $M_w = 6.75$ (Figure 1), and erosion is optimal around this break. Thus, with a Gutenberg-Richter distribution, the long-term cumulative landsliding and its uncertainty are dominated by the events between M_w 6.5 and 7, which we model in greater number as we increase M_wX, considering larger populations of earthquakes. The uncertainty (i.e., standard deviation) on the long-term cumulative landslide volume is about 33%, 17%, and 8%, for a fault with $M_wX = 7.0$, 7.5, and 8.0, respectively. In any case, we find that the long-term volume balance scaling with moment is similar to the one of the repeated

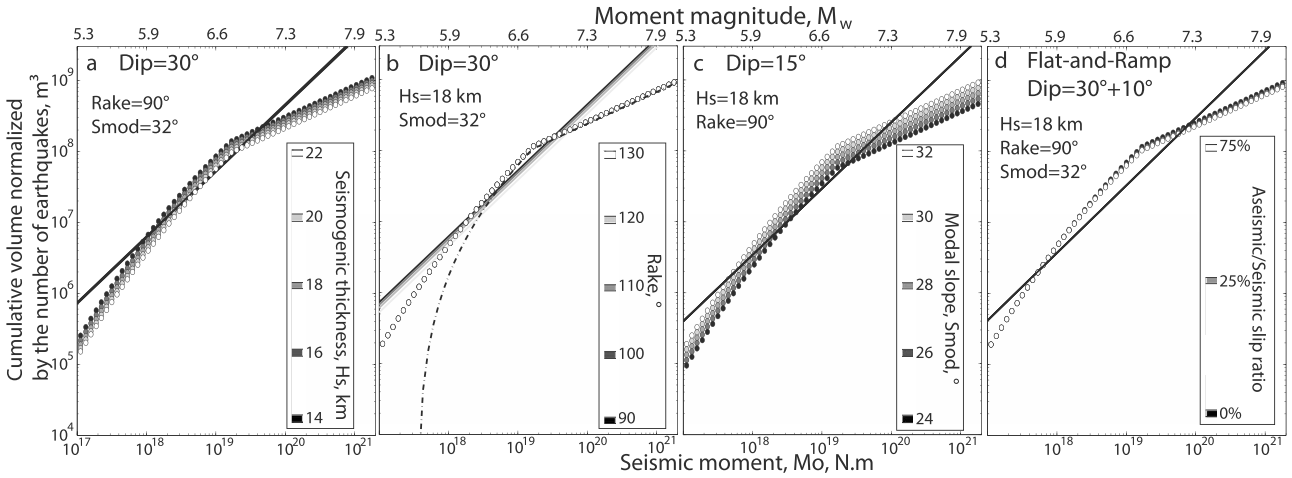

Figure 2. Cumulative volume (or mass) of landslide or uplifted rock, divided by the number of earthquakes in the sequence, for repeating earthquakes of a given seismic moment or magnitude. Four fault geometries are considered, a 30° dip thrust with varying seismogenic thickness, (a) Hs, or (b) rake, (c) a 15° dipping thrust with varying modal slope, and (d) a flat and ramp thrust (10° and 30° dipping, respectively) with a varying ratio of aseismic/seismic slip on the flat portion (see supporting information S1). For reference, the dashed line in Figure 2b shows the total volume of landslide caused by a single earthquake with a mean asperity depth of 9 km.

earthquake scenario, but with a wider range of magnitudes leading to erosive earthquakes. This is due to the large number of net erosive earthquakes of $M_w \sim 7$, the effect of which must be overcome by a few $M_w \sim 8$ earthquakes with a positive volume change to yield an overall increase in topographic volume.

Even in steep, landslide-prone landscapes with modal slopes around 32°, single faults with a dip of 30° never produce erosive earthquakes unless they have a strike-slip component or the seismogenic layer is thin (Figures 2 and 3). However, earthquakes on such faults would break a seismogenic layer of thickness 18 km in its entirety at magnitude M_w 7.6. Under these conditions larger earthquakes would not follow the length and width scaling reported by *Leonard* [2010], suggesting that earthquake size and geometry may covary and that $M_w > 7.6$ earthquakes may originate most commonly on gently dipping or flat and ramp faults. For steep landscapes, and especially with a Gutenberg-Richter scenario, we observe that gentle dipping faults and faults with flat and ramp geometry are dominated by erosion unless the fault system can generate earthquakes with M_w 7.8–8, requiring a fault length of about 150–200 km (Figure 3). Even larger earthquakes would be necessary for a positive long-term mass balance if some amount of strike-slip occurred.

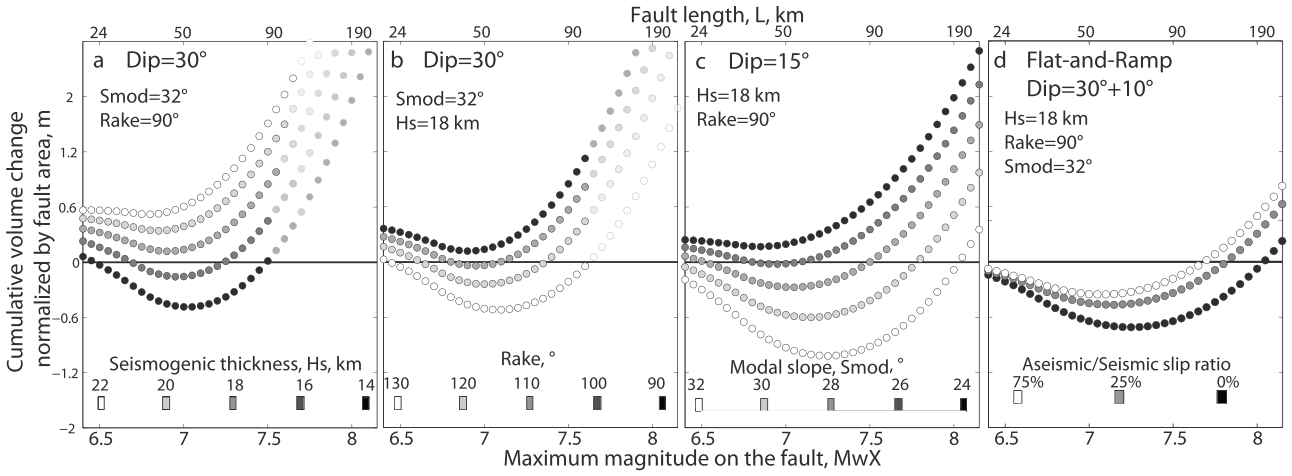

Figure 3. Long-term mass balance for a Gutenberg-Richter distribution of earthquake on a master fault of length L and maximum magnitude M_wX. Same scenarios as in Figure 2. Transparent symbols indicate unrealistic setting where the fault width reaches depth beyond the seismogenic thickness, Hs.

6. Discussion and Conclusions

We have modeled the mass balance of earthquakes by comparing the coseismic surface deformation with the volume of earthquake-triggered landslides, accounting for the seismic source depth and topographic sensitivity. In contrast to previous studies that have not considered the specifics of faulting and topography, we have found that earthquakes with a net erosive effect are not those with a large magnitude above M_w 8 but rather those with intermediate magnitudes between M_w 6.3 and 7.3. For deeper earthquakes and/or landscapes with gentle topography this range may narrow or disappear. Our model predicts that earthquakes deeper than 15 km or under landscapes with topographic modal slopes less than 20° are always constructive. We also modeled the cumulative mass balance of a fault with repeating earthquakes of similar magnitude and a fault with earthquakes following a Gutenberg-Richter distribution. In steep landscapes, we found that faults with repeating earthquakes will systematically be constructive as soon as these earthquakes reach $M_w \sim 7$–7.3, that is when the rupture length reaches 50 to 70 km. In contrast, faults with earthquakes with a Gutenberg-Richter distribution may remain dominated by erosion until they can generate earthquakes of M_w 8 or more, which requires rupture lengths in excess of 150 km. This is especially so if they dip gently or have a flat and ramp geometry, as expected for a seismogenic layer with thickness ~18 km [*Leonard*, 2010]. Such faults, which are common in fold and thrust belts, may limit orogenic growth until the fault system has grown enough to produce very large earthquake ($M_w > 8$), when net topographic growth can resume.

Our model has important limitations. First, we have not considered the isostatic rebound, which would occur due to the removal of any substantial amount of landslide debris from the uplifted topography. As previously discussed, isostasy is certainly an important part of the problem but it is largely underconstrained because we do not know the rate at which the landslide debris is exported nor if it is redeposited close to or distant from the affected topography [*Molnar*, 2012; *Densmore et al*., 2012]. Moreover, the elastic thickness that sets the length scale over which the rebound is distributed varies with the geographic location [e.g., *Jordan and Watts*, 2005]. The order of magnitude of the isostatic compensation in the case of the 2008 Wenchuan earthquake was estimated to 25–40%, assuming an elastic thickness of 20–40 km and landslide erosion distributed over 50 km across the fault [*Densmore et al*., 2012]. For most of the large earthquakes studied by *Marc et al.* [2016], intense landsliding was limited to ~30 km away from the seismogenic fault, although some earthquakes, such as the Wenchuan 2008 earthquake, have triggered significant landsliding farther afield. Further, the area affected could be much smaller for earthquakes of M_w 6–6.5. With uniform effective elastic thickness this would reduce the amount of isostatic compensation within the eroded area. Although isostatic compensation may change the sign of the earthquake mass balance where the sum of surface uplift and erosion is relatively small, our findings remain generally robust away from these cusps. For example, in settings where M_w 6.5–7 earthquakes induce 2 to 3 times more erosion than uplift the mass balance would remain negative even after accounting for 25–40% of isostatic rebound (Figure 2).

Further, we have neglected complexities such as aseismic slip, interseismic strain, and interactions with neighboring faults. Earthquake on neighboring faults may be close enough to cause uplift and/or landsliding in the topography above the fault in question and possibly also to affect the way earthquake magnitudes on that fault are distributed in time. Therefore, depending on the setting, seismic activity on neighboring faults can shift the long-term mass balance of a fault in any direction. For thrust fault, coseismic deformation is compensated to a degree by near-fault interseismic strain due to elastic loading or postseismic relaxation. This reduces both the amount of uplift and subsidence and leaves a net uplift similar to or smaller than the coseismic volume change we have computed [*Simpson*, 2015]. Numerical simulations indicate that plastic effects are minor [*Simpson*, 2015], suggesting that our results are unlikely to change fundamentally when interseismic deformation and/or an elastoplastic behavior are included. Finally, aseismic slip on a fault would build as much topography as coseismic slip but without the associated landsliding, and the computed earthquake-induced landsliding should be corrected for the coupling fraction. As the volume of coseismic landsliding is never more than 2–3 times that of coseismic uplift, faults with a coupling less than 0.5 should always build topography over the long term. However, examples of such faults are rare, (e.g., the Longitudinal Valley fault in Taiwan [*Avouac*, 2015]), and our treatment likely applies to most settings.

Finally, we have neglected any progressive evolution of the topography and effects of fault growth. This is likely reasonable over 10^5 years, but not at the scale of mountain building, that is 10^6–10^7 years. The spatial and temporal extent to which earthquakes may limit topographic growth will depend on how fast the

landscape reaches a high modal slope, on the geometry of the fault and the rate and mode of fault growth, and on whether repeated or distributed earthquakes occur on it. We suggest that in order to decipher the long-term influence of faults and earthquakes on mountain building and to explore the feedbacks between erosion and fault mechanical behavior, a mechanical model describing fault and crustal properties [e.g., *Mary et al*., 2013] would need to be effectively coupled with a landscape evolution model characterizing topography and incorporating earthquake-induced landsliding [cf. *Steer et al*., 2014]. Short of this full geodynamic approach, our mass balance model indicates that incipient faulting in a relatively gentle landscape will always lead to the construction of topography because coseismic landsliding is limited by the steepness of that topography, whatever the fault and earthquake size. However, as topography rises and steepens, the intermediate size earthquakes will quickly become destructive, limiting the rate of mountain building and eventually halting net mountain growth. During a certain period such faults and associated topography may continue to expand laterally, while their average topography is reduced. But when faults become large enough to produce earthquakes of $M_w > 7.8$–8.2, effective mountain building could resume. Therefore, our study does not challenge the role of earthquakes as a key mechanism of mountain building. Rather, it demonstrates that earthquakes are ambivalent agents, which may limit topographic growth during a given period or in a certain part of a mountain belt. For example, historical records attest that very large continental earthquakes ($M_w > 8.3$) have occurred relatively frequently on faults bounding the Himalayas [e.g., *Bollinger et al*., 2014], and the earthquake sequences likely drive topographic growth. In contrast, in many smaller mountain belts such as Taiwan, Papua New Guinea, or the mountain ranges flanking Tibet to the north, such large faults may be absent and the average topographic growth may be limited rather than supported by earthquakes.

Acknowledgments

This manuscript is based on results computed from a numerical model and not on data obtained elsewhere. The authors have no conflict of interest to declare. O.M. was funded by a fellowship in the EU Marie-Curie Initial Training Network TOPOMOD, project number 264517. The authors have no conflict of interest with the presented work. O.M. is grateful to Francois Beauducel for making available a Matlab routine solving the Okada analytical equations and to Mehdi Nikkhoo for help on the topographic effects in Okada simulation. The authors thank Alex Densmore and Ken Ferrier for their in-depth and constructive reviews that helped clarify and strengthen this manuscript, and Andrew Newman for his insightful comments and its efficient handling of the manuscript.

References

Avouac, J.-P. (2007), 6.09 Dynamic processes in extensional and compressional settings—Mountain building: From earthquakes to geological deformation, in *Treatise on Geophysics*, edited by E.-C. G. Schubert, pp. 377–439, Elsevier, Amsterdam.

Avouac, J.-P. (2015), From geodetic imaging of seismic and aseismic fault slip to dynamic modeling of the seismic cycle, *Annu. Rev. Earth Planet. Sci.*, *43*(1), 233–271, doi:10.1146/annurev-earth-060614-105302.

Avouac, J.-P., L. Meng, S. Wei, T. Wang, and J.-P. Ampuero (2015), Lower edge of locked Main Himalayan Thrust unzipped by the 2015 Gorkha earthquake, *Nat. Geosci.*, *8*, 708–711, doi:10.1038/ngeo2518.

Baltay, A. S., and T. C. Hanks (2014), Understanding the magnitude dependence of PGA and PGV in NGA-West 2 data, *Bull. Seismol. Soc. Am.*, *104*(6), 2851–2865, doi:10.1785/0120130283.

Barlow, J., I. Barisin, N. Rosser, D. Petley, A. Densmore, and T. Wright (2015), Seismically-induced mass movements and volumetric fluxes resulting from the 2010 $M_w = 7.2$ earthquake in the Sierra Cucapah, Mexico, *Geomorphology*, doi:10.1016/j.geomorph.2014.11.012.

Bollinger, L., S. N. Sapkota, P. Tapponnier, Y. Klinger, M. Rizza, J. Van der Woerd, D. R. Tiwari, R. Pandey, A. Bitri, and S. Bes de Berc (2014), Estimating the return times of great Himalayan earthquakes in eastern Nepal: Evidence from the Patu and Bardibas strands of the Main Frontal Thrust, *J. Geophys. Res. Solid Earth*, *119*, 7123–7163, doi:10.1002/2014JB010970.

Boore, D. M., and G. M. Atkinson (2008), Ground-motion prediction equations for the average horizontal component of PGA, PGV, and 5%-damped PSA at spectral periods between 0.01 s and 10.0 s, *Earthq. Spectra*, *24*(1), 99–138, doi:10.1193/1.2830434.

Densmore, A. L., R. N. Parker, N. J. Rosser, M. de Michele, L. Yong, H. Runqiu, S. Whadcoat, and D. N. Petley (2012), Reply to 'Isostasy can't be ignored', *Nat. Geosci.*, *5*(2), 83–84, doi:10.1038/ngeo1385.

Gutenberg, B., and C. Richter (1954), *Seismicity of the Earth and Associated Phenomena*, Princeton Univ. Press, Princeton, N. J.

Hovius, N., P. Meunier, C. W. Lin, H. Chen, Y. G. Chen, S. Dadson, M. J. Horng, and M. Lines (2011), Prolonged seismically induced erosion and the mass balance of a large earthquake, *Earth Planet. Sci. Lett.*, *304*(3), 347–355, doi:10.1016/j.epsl.2011.02.005.

Jordan, T. A., and A. B. Watts (2005), Gravity anomalies, flexure and the elastic thickness structure of the India-Eurasia collisional system, *Earth Planet. Sci. Lett.*, *236*(3–4), 732–750, doi:10.1016/j.epsl.2005.05.036.

Keefer, D. K. (1994), The importance of earthquake-induced landslides to long-term slope erosion and slope-failure hazards in seismically active regions, *Geomorphology*, *10*(1–4), 265–284, doi:10.1016/0169-555X(94)90021-3.

Khazai, B., and N. Sitar (2004), Evaluation of factors controlling earthquake-induced landslides caused by Chi-Chi earthquake and comparison with the Northridge and Loma Prieta events, *Eng. Geol.*, *71*(1–2), 79–95, doi:10.1016/S0013-7952(03)00127-3.

King, G. C. P., R. S. Stein, and J. B. Rundle (1988), The growth of geological structures by repeated earthquakes 1. Conceptual framework, *J. Geophys. Res.*, *93*(B11), 13,307–13,318, doi:10.1029/JB093iB11p13307.

Le Béon, M., J. Suppe, M. K. Jaiswal, Y.-G. Chen, and M. E. Ustaszewski (2014), Deciphering cumulative fault slip vectors from fold scarps: Relationships between long-term and coseismic deformations in central Western Taiwan, *J. Geophys. Res. Solid Earth*, *119*, 5943–5978, doi:10.1002/2013JB010794.

Leonard, M. (2010), Earthquake fault scaling: Self-consistent relating of rupture length, width, average displacement, and moment release, *Bull. Seismol. Soc. Am.*, *100*(5A), 1971–1988, doi:10.1785/0120090189.

Li, G., A. J. West, A. L. Densmore, Z. Jin, R. N. Parker, and R. G. Hilton (2014), Seismic mountain building: Landslides associated with the 2008 Wenchuan earthquake in the context of a generalized model for earthquake volume balance, *Geochem. Geophys. Geosyst.*, *119*, 5943–5978, doi:10.1002/2013GC005067.

Marc, O., N. Hovius, P. Meunier, T. Gorum, and T. Uchida (2016), A seismologically-consistent expression for the total area and volume of earthquake-triggered landsliding, *J. Geophys. Res. Earth Surf.*, *121*, doi:10.1002/2015JF003732.

Mary, B. C. L., B. Maillot, and Y. M. Leroy (2013), Predicting orogenic wedge styles as a function of analogue erosion law and material softening, *Geochem. Geophys. Geosyst.*, *14*, 4523–4543, doi:10.1002/ggge.20262.

Meunier, P., N. Hovius, and A. J. Haines (2007), Regional patterns of earthquake-triggered landslides and their relation to ground motion, *Geophys. Res. Lett.*, *34*, L20408, doi:10.1029/2007GL031337.

Meunier, P., T. Uchida, and N. Hovius (2013), Landslide patterns reveal the sources of large earthquakes, *Earth Planet. Sci. Lett.*, *363*, 27–33, doi:10.1016/j.epsl.2012.12.018.

Molnar, P. (2012), Isostasy can't be ignored, *Nat. Geosci.*, *5*(2), 83–83, doi:10.1038/ngeo1383.

Okada, Y. (1985), Surface deformation due to shear and tensile faults in a half-space, *Bull. Seismol. Soc. Am.*, *75*(4), 1135–1154.

Parker, R. N., A. L. Densmore, N. J. Rosser, M. De Michele, Y. Li, R. Huang, S. Whadcoat, and D. N. Petley (2011), Mass wasting triggered by the 2008 Wenchuan earthquake is greater than orogenic growth, *Nat. Geosci.*, *4*(7), 449–452, doi:10.1038/NGEO1154.

Ruiz, S., E. Kausel, J. Campos, G. R. Saragoni, and R. Madariaga (2011), Identification of high frequency pulses from earthquake asperities along Chilean Subduction Zone using strong motion, *Pure Appl. Geophys.*, *168*(1–2), 125–139, doi:10.1007/s00024-010-0117-x.

Simpson, G. (2015), Accumulation of permanent deformation during earthquake cycles on reverse faults, *J. Geophys. Res. Solid Earth*, *120*, 1958–1974, doi:10.1002/2014JB011442.

Steer, P., M. Simoes, R. Cattin, and J. B. H. Shyu (2014), Erosion influences the seismicity of active thrust faults, *Nat. Commun.*, *5*, doi:10.1038/ncomms6564.

Yuan, R.-M., Q.-H. Deng, D. Cunningham, C. Xu, X.-W. Xu, and C.-P. Chang (2013), Density distribution of landslides triggered by the 2008 Wenchuan earthquake and their relationships to peak ground acceleration, *Bull. Seismol. Soc. Am.*, *103*(4), 2344–2355, doi:10.1785/0120110233.